Development of highly efficient, renewable and durable alginate composite aerogels for oil/water separation

Jiandong Zhuang,†*[a] Juguo Dai,†[a] Seyed Hamidreza Ghaffar,[b] Yiyun Yu,[a] Qinfen Tian,[a] and Mizi Fan [a,b]

a College of Materials Engineering, Fujian Agriculture and Forestry University, Fuzhou, 350002, China. E-mail: jdzhuang@gmail.com

b College of Engineering, Design and Physical Science, Brunel University London, UB8 3PH, Uxbridge, United Kingdom

† These two authors contribute equally and are co-first authors.

Abstract

To valorize the naturally abundant biomass, bio-composites made of biomass and functional nano-materials have attracted a great deal of attention. By incorporating alginate with TiO_2/RGO nanocomposites, TiO_2/RGO/Alginate composite (TRGA) aerogels are fabricated via a facile freeze-drying method. TiO_2/RGO nanocomposites can effectively improve the surface roughness and mechanical performance of ~~aerogel~~ alginate-based matrix, and provide the aerogels with light-driven self-cleaning ability. Without further chemical modification, the as-fabricated TRGA aerogel shows: i) collective underwater superoleophobicity (θ_{oil} > 150º for various oils), ii) effective oil/water separation performance (9.76 $L \cdot m^{-2} \cdot s^{-1}$ water permeate flux and 99.96% separation efficiency) and iii) excellent light-induced recyclability. With light-driven self-cleaning ability, the continuously deteriorated separation performance of aerogel can be easily renewed, and maintain an effective oil/water separation performance even after 120 cycles. Benefiting from its facile fabrication and excellent properties, the developed aerogel can be a promising candidate for practical oil/water separation in marine oil spill clean-up applications.

Keywords: TiO_2/RGO/Alginate composite aerogels; Underwater superoleophobicity; Oil/water separation; Light-driven renewability; Environmental friendly; Long-term stability.

1. Introduction

The oil spills accidents and oily sewage discharge have caused severe damages to the environment and ecological system, and effective dealing with these issues has become a matter of global concern [1-3]. Traditional techniques [4], such as oil skimming, flotation, and mechanical collection, have always suffered from complicated operation procedures, high energy consumption, and low separation efficiency. In recent years, functional materials with outstanding wettability have attracted considerable attention. Generally, the special wettability materials for oil/water separation can be divided into two categories[5]: (1) superhydrophobic/superoleophilic (oil-removal) materials [6], and (2) superhydrophilic/superoleophobic (water-removal) materials [7]. Among them, three-dimensional (3D) aerogels, which possess extremely low densities and abundant micro pores, have been well developed and used as either oil-removal (absorbents) or water-removal (filters) materials in oil/water separation [8-10]. As compared with the superhydrophobic/superoleophilic (oil-removal) aerogels, the fabrication process of the superhydrophilic aerogels is far more convenient, low-cost and environmental-friendly, as there is no need for expensive surface modifying agents and complicated modification processes [11-14]. However, no matter which kind of aerogels is used, the continuous decline in service performance (flux and efficiency) seems to be unavoidable due to the unceasing accumulation of foulants on the surface of aerogels. Therefore, development of easily fabricated, renewable and high efficient oil/water separation aerogel filters remains a serious challenge.

Recently, novel superhydrophilic alginate-based composites, using the abundant natural biocompatible polysaccharides yielded from brown sea algae as raw material, have gained considerable interest in the field of oil/water separation [15-18]. Alginate is a unbranched

polysaccharide consisting of two basic building blocks, G-blocks (α-L-guluronic acid units) and M blocks (β-D-mannuronic acid units), linearly linked together by 1-4 linkages [19]. Using divalent cations (except Mg^{2+}) as the cross-linking agent, a stable alginate hydrogel can easily be formed and then converted to superhydrophilic aerogel [20-22]. In our previous study [15], TiO_2/Alginate composite aerogels have been fabricated successfully, and the results also prove that the composite aerogels possess a high performance in oil/water separation and sewage photocatalytic remediation. However, yet two essential issues need to be solved. Firstly, the low mechanical strength of alginate aerogel seriously influences its long-term service performance. Secondary, the wideband gap and low quantum efficiency of TiO_2 would confine the visible-light-driven photocatalysis and self-cleaning performance of composite aerogel [23-25].

As two dimensional (2D) carbon materials, graphene and its derivatives have received intensive attentions in various application fields due to their remarkable physicochemical properties. Chemically exfoliated 2D graphene oxide (GO) nanosheet, which possesses large specific surface area, numerous oxygen-containing functional groups and outstanding electronic conductivity, has been proved to be an appropriate supporting materials for photocatalysts loading and performance improvement [26, 27]. Additionally, excellent mechanical properties, high aspect ratio and good process-ability, also make the GO nanosheets an attractive building block/reinforcing filler to improve mechanical properties of aerogel materials [28, 29].

In this paper, multifunctional aerogels with high mechanical strength are fabricated by incorporating TiO_2/RGO nanocomposites with alginate matrix through a cheap and non-toxic ionic cross-linking method combined freeze-drying. The characteristics of the as-prepared TiO_2/RGO/Alginate (TRGA) composite aerogel, including morphostructure, oil and water wettability,

oil/water separation flux and efficiency, service and renewable performance are subsequently analyzed and interpreted in detail. It is believed that this renewable and high-efficient TRGA aerogels can present a novel pathway for oil/water purification.

2. Experimental section

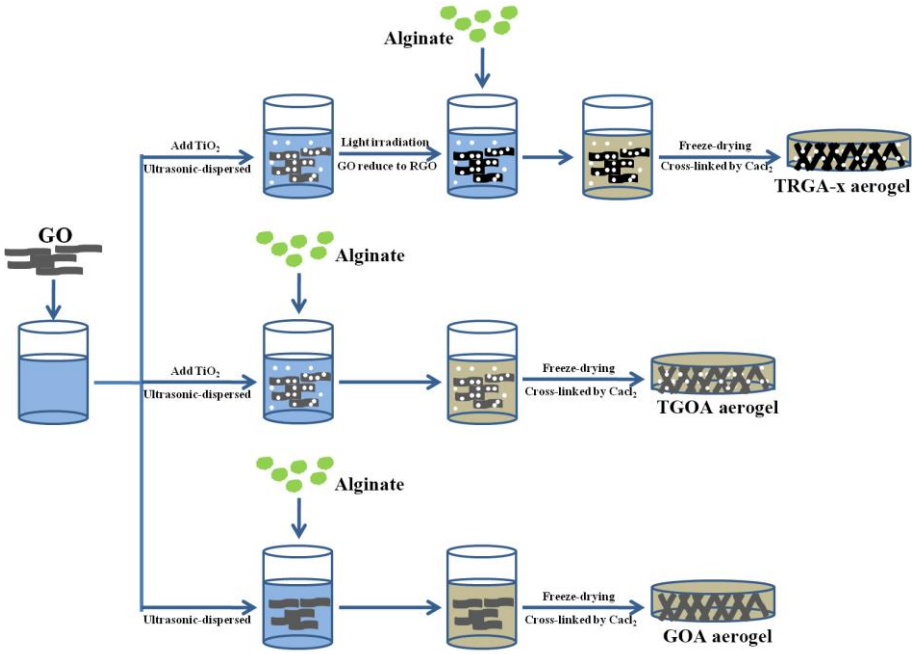

Scheme1. Schematic representation of TRGA-x, TGOA and GOA aerogels fabrication.

Materials. Sodium alginate (M/G ratio ≈ 1.56, MW: 80~120 kDa) was purchased from Shanghai Macklin Biochemical Ltd. Calcium chloride ($CaCl_2$) of laboratory grade from Xilong Chemical Ltd. P25 (nano-scale TiO_2 powder, surface area 50 m^2/g, particle size 20~30 nm) was purchased from Degussa AG of Germany. Graphene oxide (GO) was purchased from Shanghai Ashine Technology Development Ltd. All of other analytical chemicals were purchased from Aladdin, and used as received without further purification. Deionized water was used throughout the experiment.

Preparation of TRGA aerogels. The TRGA aerogel (x means the mass ratio amount of GO to Alginate is x:100) is prepared by incorporating TiO_2/RGO nanocomposites with alginate matrix, and the fabrication process is shown in **Scheme 1**. The mass ratio amount of GO to TiO_2 is controlled by

changing the additive amount of GO during the synthesis process of TiO_2/GO nanocomposites. Typically, 0.1g commercial TiO_2 (P25) is ultrasonic-dispersed in 100mL GO suspension solution (0.1 g/L). Then the mixed suspension is irradiated under UV lamps (365 nm) for 1.5h to obtain TiO_2/RGO homogeneous dispersion solution. Subsequently, 1g sodium alginate is dissolved in the aforementioned suspension to obtain uniform TiO_2/RGO/Alginate mixture. The mixture is casted into a petri dish, frozen and lyophilized in a freeze dryer (LyoBeta 3PS, Telstar, Spain) at -10 ºC, 500μbar for 24h. The obtained aerogel is further consolidated using the Ca^{2+} induced cross-linking process. After consolidation and rinsing, the gel is freeze-dried again to achieve the TRGA-1 aerogel (the mass ratio amount of TiO_2:GO:Alginate is 10:1:100). According to the same methodology, the TGOA aerogel (without GO reducing process), GO/Alginate aerogel (GOA, without TiO_2), TRGA-0.5 (TiO_2:GO:Alginate is 10:0.5:100) and TRGA-5 aerogels (TiO_2:GO:Alginate is 10:5:100) are also fabricated for comparison.

Characterization. The crystalline phase of the as-prepared samples were identified by X-ray diffraction (Rigaku, Ultima IV) operating with Cu Kα radiation. After sputter coating with gold, the microstructures of aerogels were investigated in a Hitachi SU8000 field-emission scanning electron microscope (FE-SEM). Raman investigations were also carried out on an inVia reflex Raman spectrophotometer (Renishaw, UK). The pore size was measured by the American Autopore type III 9420 automatic mercury intrusion porosimetry. The wettability of as-prepared aerogels in air and underwater was characterized by a liquid drop shape analysis system (SPCA-1 HARKE, China). The procedural detail of the oil/water separation performances tests are elaborated in the Supporting information (SI-1).

3. Results and Discussion

The phase compositions and morphologies

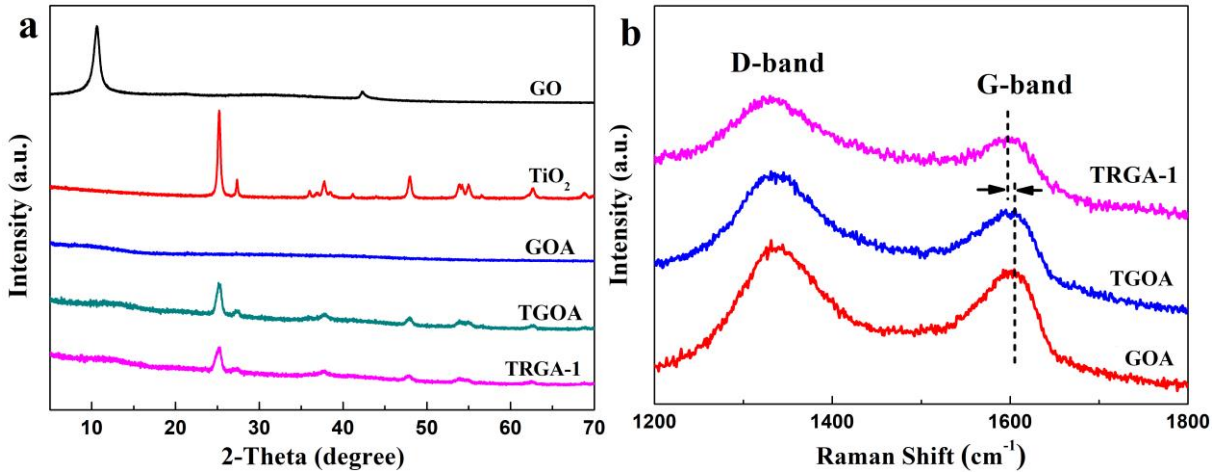

Figure 1. (a) XRD patterns and (b) Raman spectra of the as-prepared samples.

The XRD patterns of the as-prepared aerogels are shown in **Figure 1a**. It is evident that graphene oxide (GO) shows a sharp peak at 2θ=10.6º. However, the characteristic diffraction peak of GO disappears in the GOA aerogel, confirming the uniform distribution of graphene oxide in alginate matrix [27, 30]. Meanwhile, for the as-prepared TiO_2-based aerogels samples (TGOA and TRGA-1), their diffraction peaks match very well with those of the commercial TiO_2, except a remarkable decrease in peak intensities, confirming that the TiO_2 NPs can be well dispersed in the alginate matrix [15].

More evidences on the reduction of GO to RGO can be obtained from the Raman results shown in **Figure 1b**. Two characteristic peaks at ~1331cm^{-1} and ~1604cm^{-1} can be ascribed to the D-band and G-band of GO, respectively. The D-band represents the disordered carbon caused by structural defects, whereas the G-band represents the stretching vibration of tangential C-C bonds [31]. Thus for RGO, the disorder extent of graphitic structures can be reflected from the D-band and G-band intensity ratio (I_D/I_G) [31, 32]. The I_D/I_G values of GOA, TGOA and TRGA-1 aerogels are calculated to be approximately 1.02, 0.93 and 1.06, respectively. The lowest I_D/I_G value of TGOA-1 sample is attributed to the strong chemical bonding between TiO_2 NPs and GO nanosheets [23]. After

photocatalytic reduction process, the Raman I_D/I_G values of TRGA-1 is evidently increased, implying an increased number of smaller graphene domains [33, 34]. Moreover, the reduction process can also lead to a red shift in G-band. As shown in **Figure 1b**, the G-band position of the TRGA-1 aerogel moves from 1604cm^{-1} (GOA and TGOA aerogels) to 1597cm^{-1}, which is closer to the value of pristine graphite, further confirming the reduction of GO.

Many studies have demonstrated that the special wettability of functional materials is governed by both microstructure and surface chemical composition [35-37]. As observed in lower magnification SEM images shown in **Figure 2**, all the as-prepared aerogels are of interconnected 3D porous structure. The highly porous structure is beneficial for the oil/water gravitational separation and the increase of separation flux [38]. Besides that, the surface roughness of the matrix is also a significant factor for the wettability of aerogels, which can consequently influence the oil/water separation efficiency. In the higher magnification SEM images shown in **Figure 2**, it can be clearly observed that the surface of GOA aerogel is smooth and there are only some slight wrinkled corrugations in the matrix. Obviously, the introduction of TiO_2 NPs, which can be uniformly disperse on the skeleton surface of aerogel, would remarkably roughen the TGOA aerogel surface. The resulted rougher surface is beneficial for the superhydrophilicity (i.e., underwater oleophobicity) of aerogels. Whereas for the TRGA-1 aerogels, its surface becomes much rougher after introducing the TiO_2/RGO nanocomposites. Due to hydrogen bonding between the TiO_2/RGO nanocomposites and the Alginate matrix, (both are rich in hydroxide groups); TiO_2/RGO nanocomposites can be anchored firmly on the Alginate matrix to improve the surface roughness of Alginate-based ~~aerogels~~ matrix.

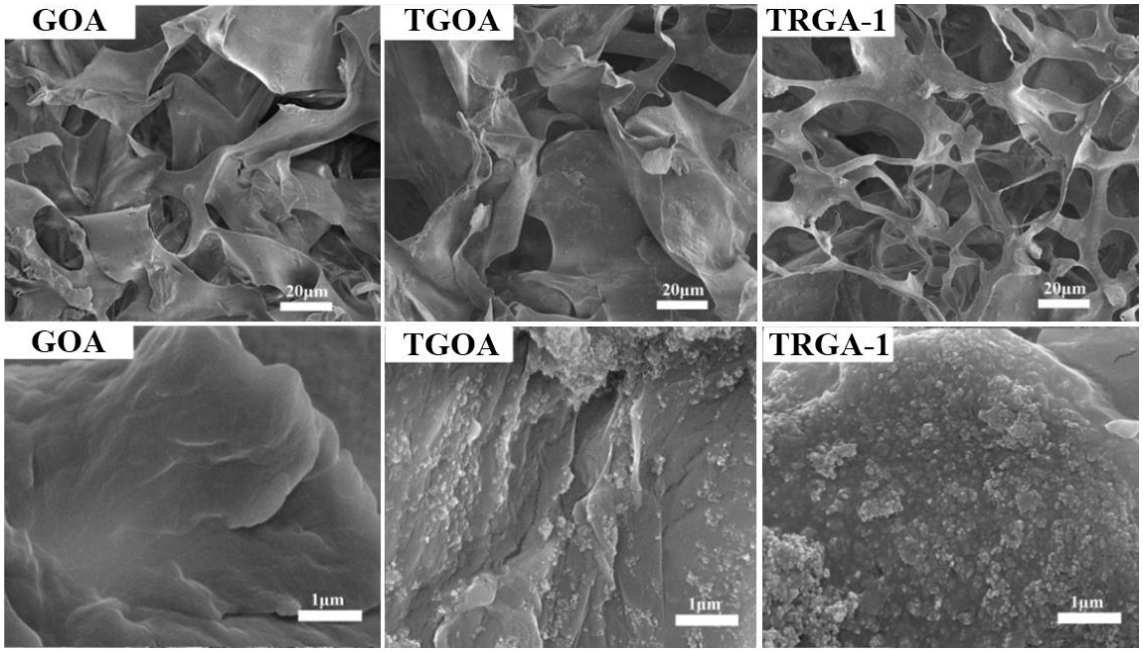

Figure 2. SEM images of GOA, TGOA and TRGA-1 aerogels

Wettability characterization

The as-prepared aerogels surface wettability is a crucial property, which governs their application in wastewater treatments. As shown in **Figure 3a**, the water (or oil) droplet can quickly spreads and penetrate into the aerogel, indicating the high surface affinity and permeability of the aerogels towards water and oil in atmospheric condition. It can therefore be concluded that due to the high content of polysaccharides and the 3D porous architecture generated in the freeze-drying process, the as-fabricated alginate-based aerogels have the desirable super amphiphilicity and excellent liquid penetration-ability, which can provide the aerogels a unique surface wettability and effective detachment capacity.

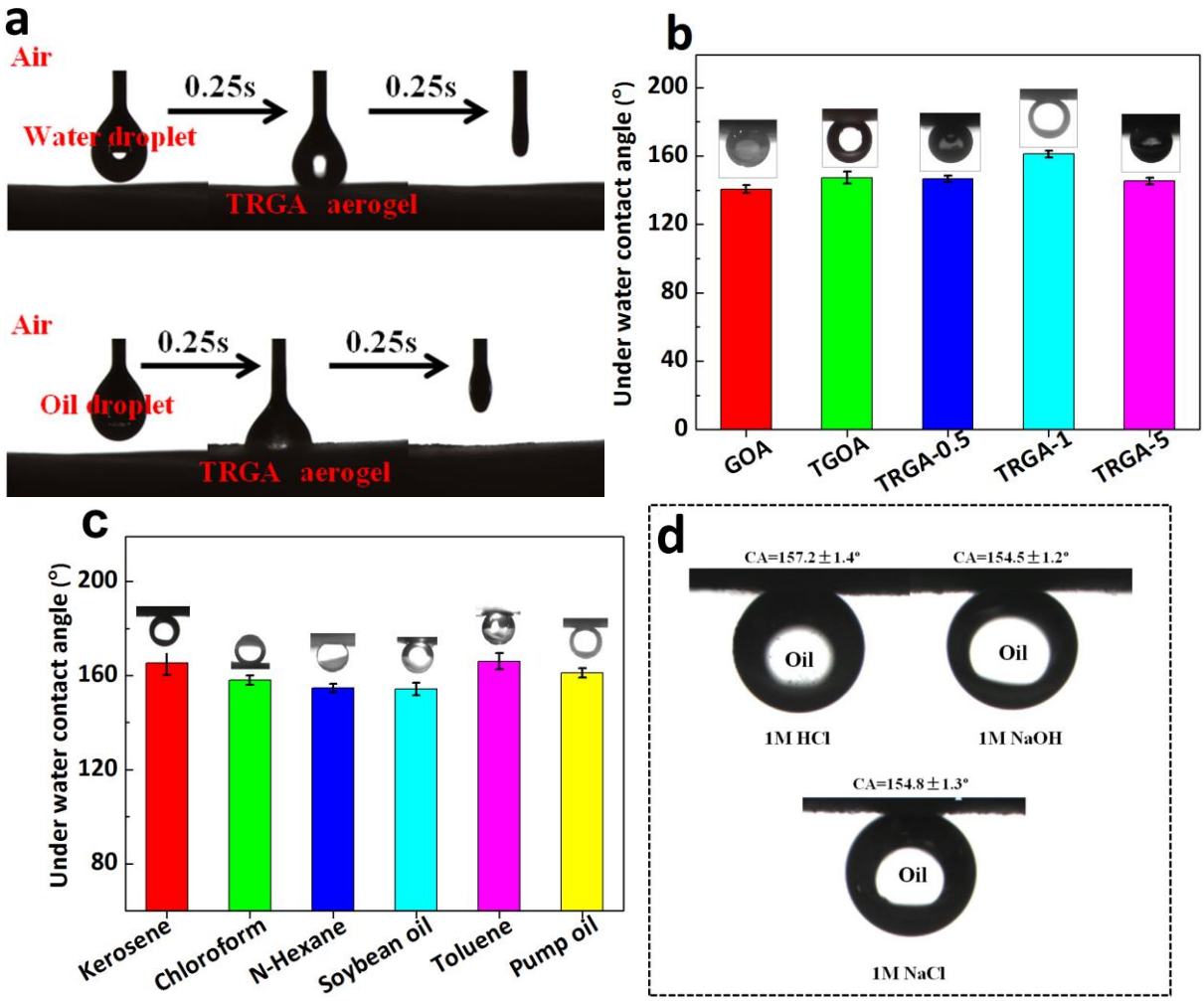

Figure 3. a) Water and oil wettability of TRGA-1 aerogel in air, b) pump oil contact angle underwater of as-prepared aerogels, c) underwater contact angles of TRGA-1 aerogel for various probing oil/organic solvents, and b) digital images of pump oil droplet over TRGA-1 aerogel in 1M HCl, NaOH and NaCl solutions.

Underwater contact angles from six different types of oil/organic solvent are further measured to investigate the aerogels' wettability characteristics in the oil/water/solid three-phase system. **Figure 3b** shows the underwater contact angles of pump oil over different aerogels and the corresponding digital photos of pump oil droplet shapes. The underwater pump oil contact angle of TGOA aerogel (147.3±3.4º) is higher than that of GOA aerogel (140.6±2.2º), proving the TiO_2 NPs caused roughen surface can enhance the underwater superoleophobicity of TGOA aerogel. This implies that roughen surface will ensure high capacity of trapping water and reinforce the oil-repellency of the aerogels. As the TRGA-1 aerogel has the roughest surface nanostructure, it displays the highest underwater contact angle for pump oil (reach up to 161.2±2º). While, further increase in the RGO content will

shelter the TiO_2 NPs and smooth the surface of aerogel matrix (**Figure S1**), leading to a lower underwater pump oil contact angle of TRGA-5 aerogel (145.2±0.1°).

Table 1. Density, pore size, flux, and underwater pump oil contact angle of the as-fabricated aerogels

Samples	Density (mg/cm^3)	Average pore size (μm)	Flux ($L \cdot m^{-2} \cdot s^{-1}$)	Underwater oil contact angle (°)
GOA	24.49	40.01	3.06±0.17	140.6±2.2
TGOA	26.45	48.35	4.53±0.39	147.3±3.4
TRGA-0.5	25.78	49.05	6.98±0.31	146.6±0.9
TRGA-1	26.88	60.91	9.77±0.27	161.2±2.0
TRGA-5	28.41	65.49	11.16±0.23	145.2±0.1

Besides the surface nano-sized roughness, the pore size could also play an important role in the underwater superoleophobicity of the aerogels. According to the previous study [38], the ideal pore size of the aerogels is approximately 60μm, otherwise the underwater superoleophobicity ($\theta_{oil} > 150°$) would be hard to realize. For the as-fabricated aerogels in this paper, the relationship between pore sizes and the contents of additives is shown in **Table 1** and **Figure S2**. It is found that by adding TiO_2 NPs, the average pore-size of GOA aerogel (~40 nm) can be slightly expanded, to be ~48 nm for the obtained TGOA aerogel. As shown in SEM images (**Figure 2**), the addition of TiO_2 NPs can remarkably increase the roughness of the alginate matrix. The rougher matrix can enhance the water trapping capacity of aerogel, and be more conducive to the formation and growth of ice crystals during the freeze-drying process, leading to expanded pores in aerogel.

Furthermore, when the GO nanosheets are reduced, the expanding effect seems to be more remarkable. It is gathered that the introduction of RGO, which possess excellent mechanical property, will greatly influence the original pore structure of the aerogels during the freeze-drying process, leading to the changes in pore sizes of aerogels [13, 39, 40]. The as-fabricated TRGA-1 aerogel shows an optimized pore size of ~60.9μm, which is nearly similar to the ideal value (60μm)

suggested. The optimized pore-size combined with rough surface microstructure provide the TRGA-1 aerogel with excellent superoleophobicity underwater.

The underwater oil-contact angles of the TRGA-1 aerogel for six typical oils/organic solvents are further measured and presented in **Figure 3c**. For various oils/organic solvents used, the measured underwater oil-contact angles of TRGA-1 are all higher than 150°, confirming the TRGA-1 aerogel is of a collective and excellent superoleophobic property underwater. Meanwhile, it is important to point out that the practical waste water environment is always harsh, e.g. the strong acidic/alkaline or high salt. To evaluate the oleophobicity and tolerability of TRGA-1 aerogel in harsh environments, the underwater pump oil contact angles were further tested in acidic (HCl), alkaline (NaOH), or high salt (NaCl) environments. As shown in **Figure 3d**, all the oil droplets over aerogels are of quasi-spherical shape, and the corresponding underwater oil contact angel is 157.2±1.4º, 154.5±1.2º, and 154.8±1.3º in 1mol/L HCl, NaOH and NaCl solutions, respectively. The stable superoleophobicity of TRGA-1 aerogel in the aforementioned corrosive liquids may be ascribed to two reasons: i) alginate is insensitive to the high ion concentration, and ii) the 3D interconnected aerogel network structure has good mechanical strength.[41]

Oil/water separation performance

Due to the excellent selective wettability and tolerability, the as-fabricated TRGA-1 aerogel could possess encouraging potentials in oil/water separation. The separation tests are carried out in an ad-hoc device to estimate the actual separation performance of TRGA-1 aerogels (**Figure S3**), where the separation process is completely driven by gravity. The oil/water mixture consists of 100mL water and 100mL pump oil (dyed by Sudan Red III into red), and the water soaked aerogel is used as a filter fixed between glass tube and suction flask. **Figure 4a** is the digital photo of the system during

oil/water separation process. When the oil/water mixture is poured into the upper tube, water can quickly permeate through the aerogel into the underneath suction flask (**Movie S1**). Noticeably, the aerogel filter selectively blocks the pump oil and no visible oil droplets can be observed in the filtered water. As illustrated in **Figure 4b**, due to the superhydrophilicity of TRGA-1 aerogel and the consequent underwater superoleophobic surface, the water will readily permeate through the water soaked aerogel filter, while the oil droplets will be repelled, retained and removed from the mixture, leading to a high-effective oil/water separation.

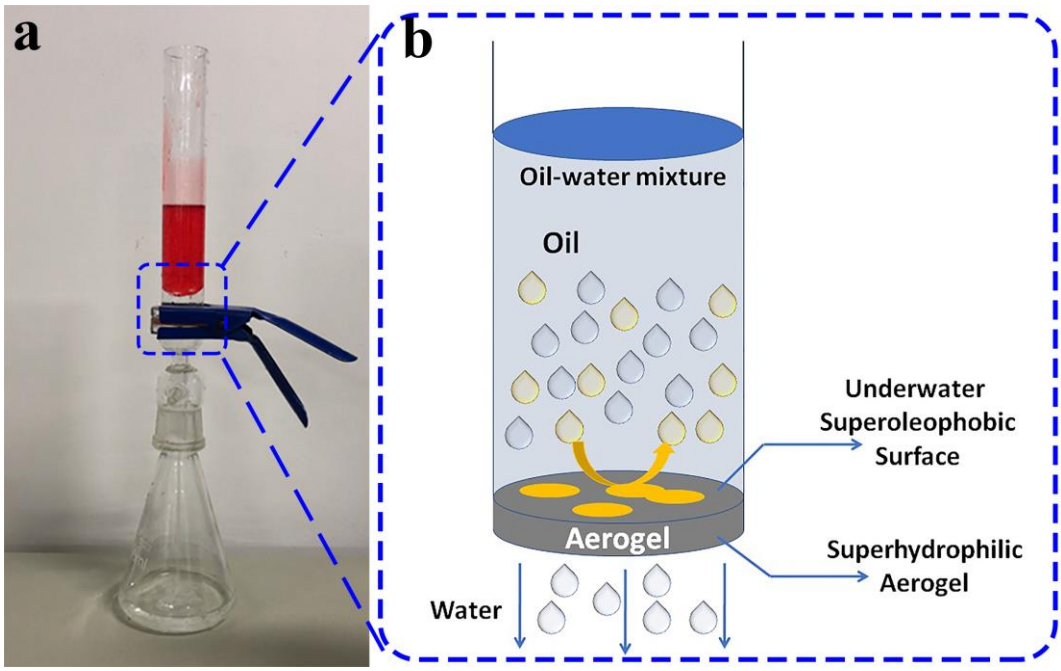

Figure 4. a) Digital photo of the TRGA-1 aerogel oil/water separation process with a self-design device, and b) illustration for the oil/water separation mechanism.

To gain a deeper understanding of the major influencing factors on the oil/water separation efficiency, the pump oil/water separation performances of different aerogels were similarly assessed. It is evident that the oil/water separation efficiency of the aerogels are closely related to their underwater oil contact angle (**Figure 5a**), and the TRGA-1 aerogel shows optimum oil/water separation efficiency (even higher than 99.96%). Evidently, the excellent oil/water separation efficiency of TRGA-1 aerogel can be mainly attributed to three unique microstructures, including the

nanoscale rough surface, the appropriate/optimized pore size and the hierarchical submerged 3D microstructure. Additionally, the water flux is also a key index to evaluate the separation performance of the filters. For the superhydrophilic aerogel filters, the water flux depends mainly on the pore size of 3D monolithic aerogel, and the larger pore size can remarkably enhance the water flux during the separation process (**Figure 5a**). For the TRGA-1 aerogel, the water flux is 9.77±0.27 $L \cdot m^{-2} \cdot s^{-1}$, meaning that this aerogel filter (with 10×10 cm^{-2} effective area) can completely separate 10 liter oil/water mixture in less than 2 minutes.

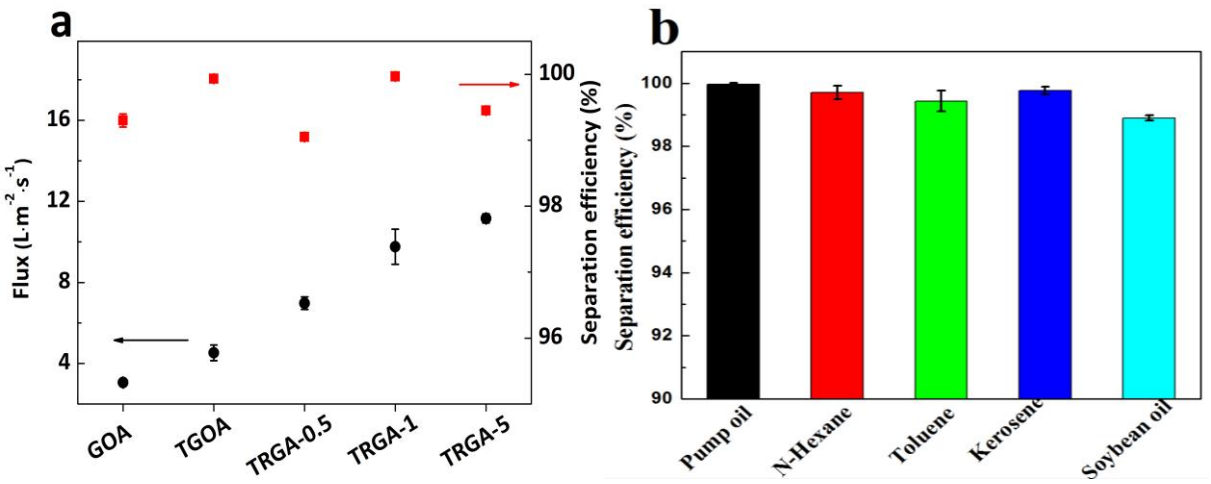

Figure 5. a) Separation efficiencies and corresponding flux of various aerogels, and b) oil/water separation efficiencies of TRGA-1 aerogel for five different oils/solvents.

To confirm the collective nature of TRGA-1 aerogel for various oil/water mixture separation, four different kinds of oil or organic solvents including n-hexane, toluene, kerosene and soybean oil were used as probing oil. As expected, all four types of oil/water mixtures were successfully separated, and the separation efficiencies are all higher than 98.9% (**Figure 5b**), indicating that the TRGA-1 aerogel has a collective and excellent oil/water separation capacity.

Antifouling and self-cleaning ability

Additionally, the as-fabricated TRGA-1 aerogel also possesses good antifouling properties from oil. The competitive process between oil and water is illustrated in **Figure 6**. As it was mentioned for

Figure 3a, the dry TRGA-1 aerogel is amphiphilic, which absorbs oil molecules while immersed in oil. Nevertheless, when the oil soaked aerogel is dipped into the water, the absorbed oil will be expelled and replaced by water due to good adsorption (**Figure 6c**). For the alginate-based aerogels, its affinity for water molecule is much higher than that for oil or organic molecules. Therefore, after being soaked by water, the water molecules will be trapped firmly in the 3D aerogel structure due to the strong hydrogen bonds between water and polysaccharide. The formed water film can spread uniformly on the aerogel surface and effectively inhibit the oil or organic pollutants to adhere, improving the aerogel filters' resistance to fouling [41, 42].

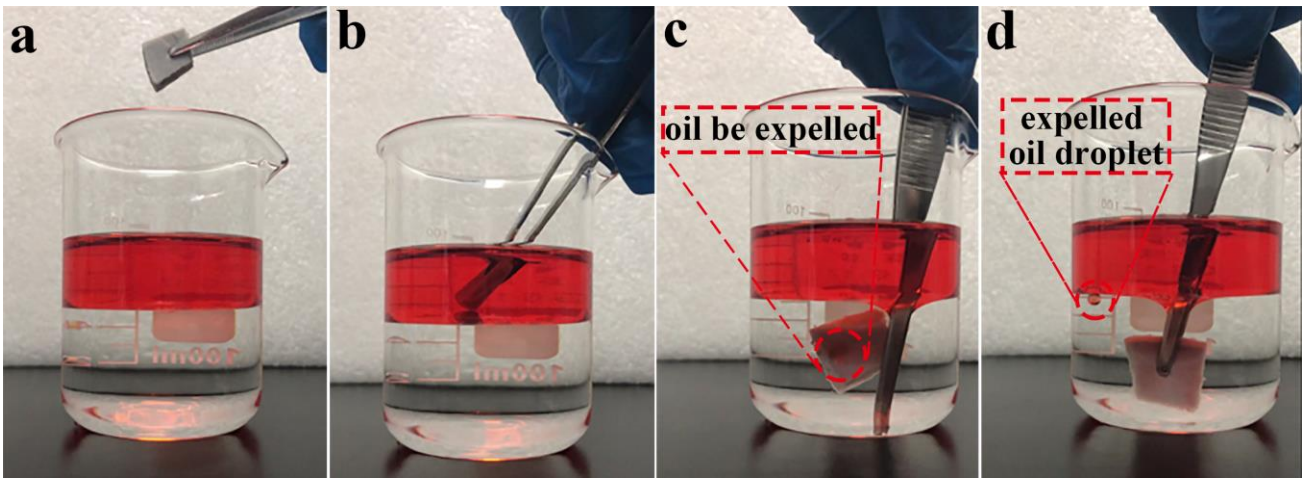

Figure 6. Competitive adsorption effect of pump oil (dyed by Sudan III) and water on the TRGA-1 aerogel.

However, during the long-term oil/water separation, the residual oil or organic pollutants will unavoidably attach on the external surface or within pores of the filters. The coalesced oil droplets accumulate over time to reverse the wettability of the aerogels from oleophobicity to oleophilic, and block the water transportation paths, leading to a serious deterioration in their separation performance and reusability [43, 44]. Therefore, self-cleaning ability is extremely important for the aerogels in practical oil/water separation applications. In this work, the introduction of TiO_2/RGO composited photocatalyst can provide the aerogels with visible-light-driven photocatalytic performance. Under light irradiation, the as-prepared TiO_2/RGO containing aerogels show efficient

photocatalytic activity and stability for organic dye (MO) decomposition (**Figure 7**).

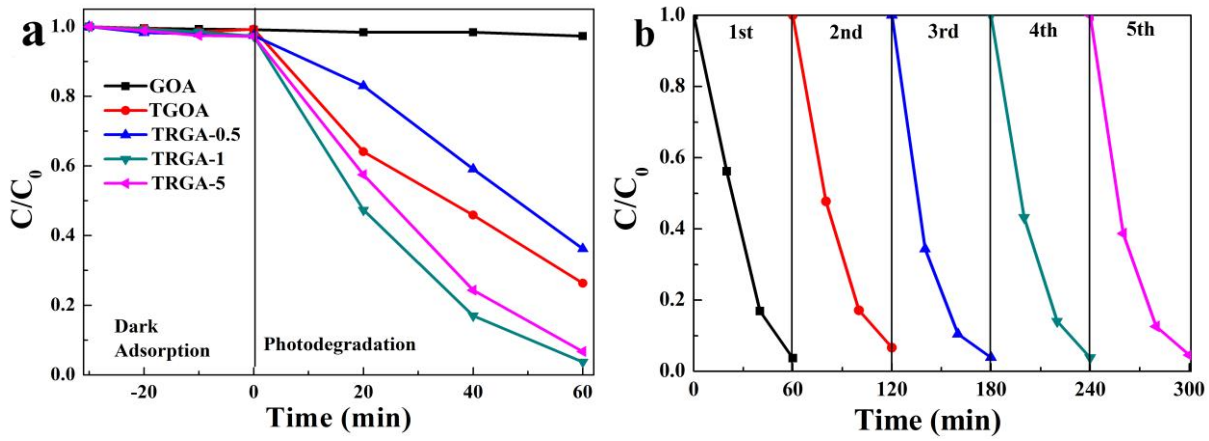

Figure 7. (a) The photodegradation efficiency of MO of various aerogels, and (b) the photocatalytic stability evaluation of TRGA-1 aerogel.

It is evidents that in the absence of TiO_2, MO is very stable with the GOA aerogel under irradiation (**Figure 7a**). While TiO_2/RGO is added, the degradation rate of MO is dramatically promoted, and the photocatalytic activities of the TRGA-x aerogels are in the descending order of TRGA-1 (96.3%) > TRGA-5 (93.3%) > TRGA-0.5 (64.8%). This result indicates that TiO_2/RGO nano-composites dispersed in alginate matrix retain a high photocatalytic activity for MO degradation. Particularly, the alginate matrix covered with TiO_2/RGO is stable against photoinduced corrosion, a common property shared by many objects coated by TiO_2. This encourages the long service life of the filter and makes the recycling of photocatalysts more convenient. The cyclic photodegradation of MO over the TRGA-1 aerogel filter was also examined to evaluate the photostability of both TiO_2/RGO nano-composites and aerogel under intensive light irradiation. As shown in Figure 7b, the TRGA-1 aerogel exhibits good photostability without any appreciable loss of photocatalytic activity even after six consecutive runs. Moreover, there is no apparent damage observed in TRGA-1 aerogel under the experimental condition, indicating the remarkable UV-aging resistance capacity. Therefore, the prepared TRGA-1 composite aerogel can overcome the recycling issues of traditional nano-photocatalyst and the issues with the environmental variability of

bio-materials, therefore, presenting a promising materials for practical applications in industry oily wastewater treatment.

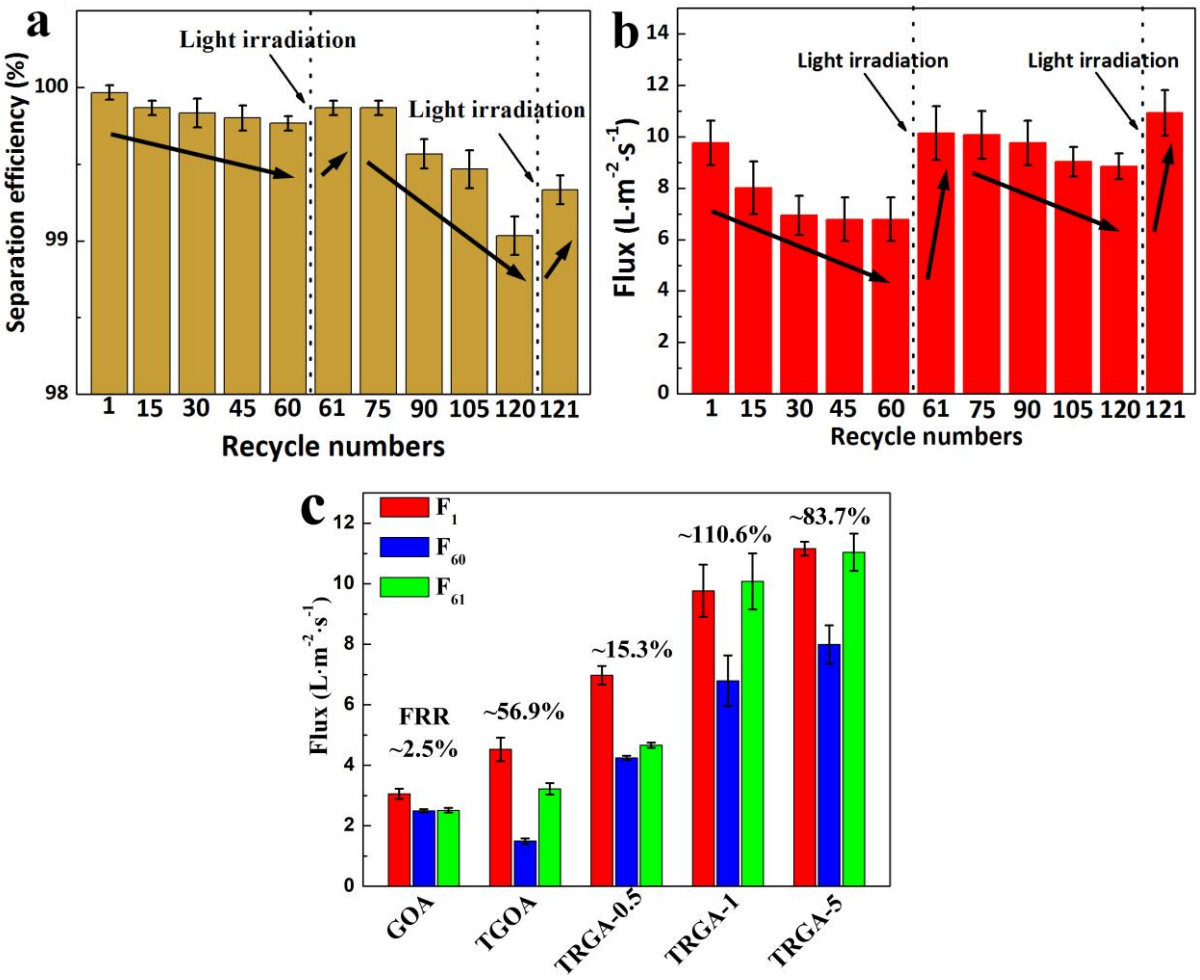

Figure 8. Changes in a) the oil/water separation efficiency, and b) the water flux of the TRGA-1 aerogel with the increased recycle times and light treatments. c) The water flux and the corresponding FRR value of various aerogels.

The self-cleaning ability of TRGA-1 aerogel could also be evaluated in the oil/water separation cycles experiments. **Figure 8** shows the changes in the oil/water separation efficiency and the water flux of the aerogels during the recycle experiments and light treatment. With the increase of cycling times, as expected, both the separation efficiency and the water flux of the TRGA-1 aerogel show a noticeable decline. As shown in **Figure 8a**, the initial separation efficiency of the TRGA-1 aerogel is near 100%, and a slight decrease (~ 0.2%) in the separation efficiency can be found after 60 times reuse cycles, which illustrates the highly stable oil-water separation performance of TRGA-1 aerogel.

After a 30 min irradiation of simulated sunlight, it is worth emphasizing that the separation efficiency of the TRGA-1 aerogel can be well recovered (to ~99.9%), indicating the good light-driven self-cleaning performance of TRGA-1 aerogel. By continuing further 60 time cycles, the separation efficiency of the same TRGA-1 aerogel exhibits a fair reduction (~0.6%), nevertheless, the light-driven recovery effect can yet be enough to enhance its oil/water separation proficiency.

Interestingly, a similar change trend can also be found in the water flux of the TRGA-1 aerogel during the cycle experiments (**Figure 8b**). For instance, the initial water flux (F_1) of the TRGA-1 aerogel is about 9.77 $L \cdot m^{-2} \cdot s^{-1}$, and after 60 times cycle separation, this value (F_{60}) decreases to ~6.79 $L \cdot m^{-2} \cdot s^{-1}$ due to the residual oil on the external surface or within pores of the filters. With 30 min irradiation of simulated sunlight, the water flux of the TRGA-1 aerogel is recovered, and the recovered flux (F_{61}, up to 10.08 $L \cdot m^{-2} \cdot s^{-1}$) is even higher than the initial water flux (F_1). The flux recovery ratio (FRR) value can be calculated by the following Equation (1):

$$V_{FRR} = (F_{61}-F_{60})/(F_1-F_{60}) \quad (1)$$

The changes in the water flux of different aerogels during the cycle experiments and their recovered flux rates (FRR) after light irradiation are presented in **Figure 8c**. It can be seen that the water flux of all the as-fabricated aerogels experience a remarkable decline after 60 times cycles. As for GOA, the F_{60} is only about 81% of the F_1 value, and the light irradiation does not work for the water flux recovery due to the absence of photocatalysts. Evidently, the introduction of TiO_2/RGO composites and the consequent light-driven recovery effect can enhance the self-cleaning performance and the reusability of the alginate-based aerogels. The light induced FRR value of the TRGA-1 aerogel can reach up to 110.6%, indicating that this aerogel easily achieves self-healing by using the light irradiation. The observed characteristics demonstrate that the TRGA-1 aerogels have

an optimum separation efficiency and long-term performance for oil/water mixtures, and can be practical for effective utilization in harsh water environment.

Limit intrusion pressure analysis

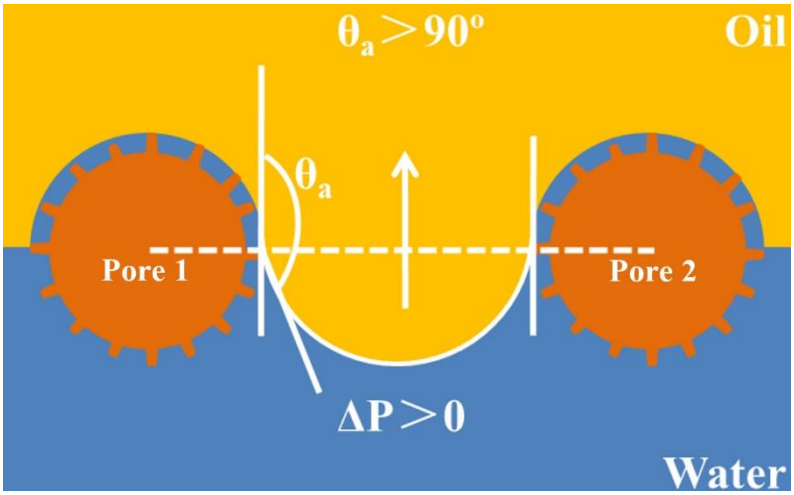

Figure 9. Schematic illustration of oil/water separation mechanism of the aerogels.

It is well known that for the amphiphilic solid materials, their difference affinities for water and oil are mainly responsible for the special surface wettability. In this work, the as-fabricated alginate-based aerogels have a strong affinity for water rather than oil or organic solvents. Thus, when the aerogels are soaked in water, the water molecules will be firmly trapped in the pores of 3D aerogel microstructure to make the aerogel surface superoleophobic [41, 45]. To illustrate the oil/water separation mechanism of the developed aerogel, the liquid wetting model is displayed in **Figure 9**. The theoretical intrusion pressure ($P_{intrusion}$), which is calculated by the following Equation (2) can explain the interaction between water and oil:

$$P_{intrusion} = 2\gamma\cos\theta_0/d \qquad (2)$$

where γ is the interfacial tension between water and oil, θ_0 is the oil contact angle, and d is the adjacent geometric peaks distance, here is approximate to the average diameter of the pores [38, 41]. Based on the equation, the underwater superhydrophilic aerogel allows spontaneous water

permeation (θ_0 is nearly 0º), and sustains a high oil intrusion pressure (θ_0 > 150º) to effectively block the oil.

The actual limit intrusion pressures of pump oil over different aerogels were also investigated, as illustrated in **Figure 10**. The GOA aerogel shows a low limit intrusion pressure (~1.55kPa) for pump oil. When TiO_2 NPs is introduced, the limit intrusion pressure of the as-fabricated TGA-1 aerogel gets a remarkable enhancement (about 26%), confirming the significant role of the surface nanoscale roughness. As expected, the TGRA-1 aerogel possesses the highest limit intrusion pressure for pump oil. It can be seen in **Figure 10b** that the pump oil column blocked by TRGA-1 aerogel has reached the maximum height of glass tube (~23.5cm), and the intrusion pressure is calculated to be higher than 2.05kPa. There is no doubt that the TRGA-1 aerogel filter would support a higher oil column if the glass tube had higher capacity.

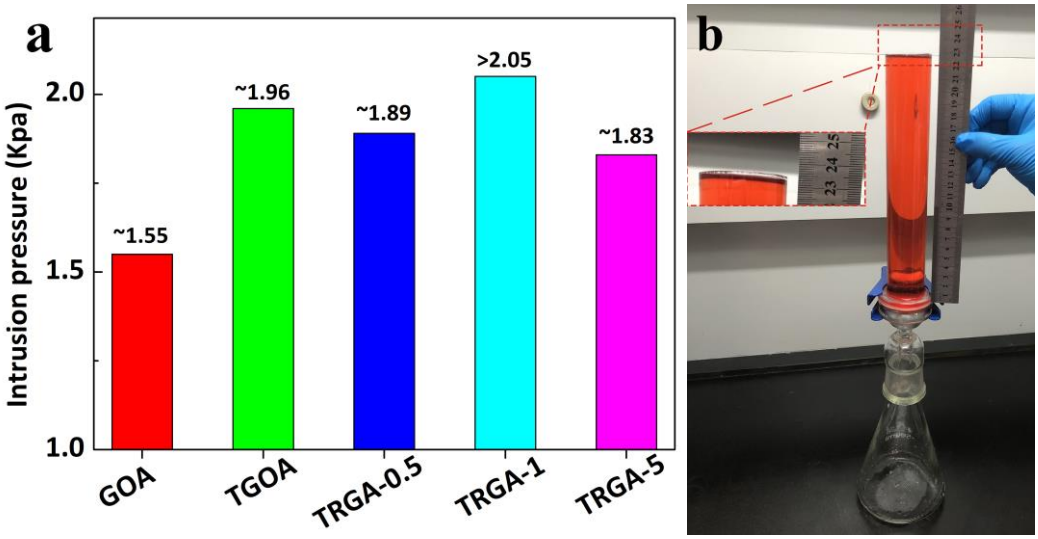

Figure 10. a) The limit intrusion pressures of pump oil over various aerogels, and b) the image of oil intrusion pressure test of TRGA-1 aerogel.

In the practical oil/water separation, a high oil column is needed to support the filtration. Therefore, the mechanical strength (especially the bending performance) is also a very important measure for the quality of the aerogel filter. As shown in **Figure S4**, the as-fabricated TRGA-1 aerogel can be bent and twisted in any direction without any apparent damage, which implies it has

excellent bending capacity. The existence of RGO nanosheets can reinforce the mechanical strength of the aerogel matrix. The RGO nanosheets reinforced honeycomb spatial structure (shown in the SEM images) will make the aerogel stronger and more flexible. Based on the results above, it is evident that the developed TRGA-1 aerogel is of excellent oil/water separation efficiency, high water permeate flux and oil intrusion pressure, good mechanical performance and remarkable tolerability.

4. Conclusions

This paper provides a new strategy and facile approach to fabricate a robust tolerant superoleophobic TiO_2/RGO/Alginate aerogel for efficient oil/water separation. The TiO_2 NPs can effectively improve the surface roughness of the aerogel matrix, and provide the aerogel with photoinduced self-cleaning ability. The RGO nanosheets reinforced 3D honeycomb spatial structure further guarantee the excellent mechanical capacity (i.e. bending and flexibility) of the TiO_2/RGO/Alginate aerogel. With excellent tolerance and underwater superoleophobicity, the as-fabricated TRGA-1 aerogel proved effective, i.e. high oil/water separation efficiency and water permeate flux, and highly recyclable, i.e. more than 60 times reuse for long-term oil/water separation in harsh environments. More importantly, the light-driven self-cleaning effect allows the TRGA-1 aerogel to maintain the high separation efficiency (~99.3%) and water permeate flux (~10.96 $L \cdot m^{-2} \cdot s^{-1}$) even after 120 cycles. These properties combined with its facile fabrication process make the TRGA-1 aerogel a promising candidate for oil/water separation in marine environments. Additionally, the results of the present work would also be beneficial for the design of new robust, high-performance filter for practical oil/water separation in marine oil spill clean-up applications.

Acknowledgments

This work is financially supported by the Program for New Century Excellent Talents in Fujian Province University (NCETFJ); Natural Science Foundation of Fujian Province (No. 2016J01207);

Youth education and scientific of Fujian Province (No. JAT170154); and Outstanding Youth Fund of Fujian Agriculture and Forestry University (No. XJQ201419, CXZX2017292).

Notes and references

[1] C.C. Wang, J.R. Li, X.L. Lv, Y.Q. Zhang, G.S. Guo, Photocatalytic organic pollutants degradation in metal-organic frameworks, Energ Environ Sci, 7 (2014) 2831-2867.

[2] Y.F. Xu, C. Zhang, P. Lu, X.H. Zhang, L.X. Zhang, J.L. Shi, Overcoming poisoning effects of heavy metal ions against photocatalysis for synergetic photo-hydrogen generation from wastewater, Nano Energy, 38 (2017) 494-503.

[3] M.A. Shannon, P.W. Bohn, M. Elimelech, J.G. Georgiadis, B.J. Marinas, A.M. Mayes, Science and technology for water purification in the coming decades, Nature, 452 (2008) 301-310.

[4] P. Li, Q. Cai, W. Lin, B. Chen, B. Zhang, Offshore oil spill response practices and emerging challenges, Marine Pollution Bulletin, 110 (2016) 6-27.

[5] Z.X. Xue, Y.Z. Cao, N. Liu, L. Feng, L. Jiang, Special wettable materials for oil/water separation, J Mater Chem A, 2 (2014) 2445-2460.

[6] H. Zhang, Z. Wang, Y. Shen, P. Mu, Q. Wang, J. Li, Ultrathin 2D Ti3C2Tx MXene membrane for effective separation of oil-in-water emulsions in acidic, alkaline, and salty environment, Journal of colloid and interface science, 561 (2020) 861-869.

[7] X. Yin, Z. Wang, Y. Shen, P. Mu, G. Zhu, J. Li, Facile fabrication of superhydrophobic copper hydroxide coated mesh for effective separation of water-in-oil emulsions, Separation and Purification Technology, 230 (2020) 115856.

[8] H. Maleki, L. Whitmore, N. Husing, Novel multifunctional polymethylsilsesquioxane-silk fibroin aerogel hybrids for environmental and thermal insulation applications, J Mater Chem A, 6 (2018) 12598-12612.

[9] H. Zhang, Y.Q. Li, Y.G. Xu, Z.X. Lu, L.H. Chen, L.L. Huang, M.Z. Fan, Versatile fabrication of a superhydrophobic and ultralight cellulose-based aerogel for oil spillage clean-up, Phys Chem Chem Phys, 18 (2016) 28297-28306.

[10] A.P. Periasamy, W.-P. Wu, R. Ravindranath, P. Roy, G.-L. Lin, H.-T. Chang, Polymer/reduced graphene oxide functionalized sponges as superabsorbents for oil removal and recovery, Marine Pollution Bulletin, 114 (2017) 888-895.

[11] B.Y.L. Tan, Z.Y. Liu, P. Gao, M.H. Tai, D.D. Sun, Oil-Water Separation Using a Self-Cleaning Underwater Superoleophobic Micro/Nanowire Hierarchical Nanostructured Membrane, ChemistrySelect, 1 (2016) 1329-1338.

[12] R. Li, C.B. Chen, J. Li, L.M. Xu, G.Y. Xiao, D.Y. Yan, A facile approach to superhydrophobic and superoleophilic graphene/polymer aerogels, J Mater Chem A, 2 (2014) 3057-3064.

[13] N. Cao, Q. Lyu, J. Li, Y. Wang, B. Yang, S. Szunerits, R. Boukherroub, Facile synthesis of fluorinated polydopamine/chitosan/reduced graphene oxide composite aerogel for efficient oil/water separation, Chem Eng J, 326 (2017) 17-28.

[14] J.W. Zeng, Z.G. Guo, Superhydrophilic and underwater superoleophobic MFI zeolite-coated film for oil/water separation, Colloid Surface A, 444 (2014) 283-288.

[15] J. Dai, Q. Tian, Q. Sun, W. Wei, J. Zhuang, M. Liu, Z. Cao, W. Xie, M. Fan, TiO2-alginate composite aerogels as novel oil/water separation and wastewater remediation filters, Compos Part B: Eng, 160 (2019) 480-487.

[16] Y.Q. Li, H. Zhang, M.Z. Fan, P.T. Zheng, J.D. Zhuang, L.H. Chen, A robust salt-tolerant superoleophobic alginate/graphene oxide aerogel for efficient oil/water separation in marine environments, Sci Rep, 7 (2017) 46379.

[17] X. Wang, M. Li, Y. Shen, Y. Yang, H. Feng, J. Li, Facile preparation of loess-coated membranes for multifunctional surfactant-stabilized oil-in-water emulsion separation, Green Chem, 21 (2019) 3190-3199.

[18] H. Zhang, Y. Shen, M. Li, G. Zhu, H. Feng, J. Li, Egg shell powders-coated membrane for surfactant-stabilized crude oil-in-water emulsions efficient separation, ACS Sustainable Chemistry & Engineering, 7 (2019) 10880-10887.

[19] C.H. Goh, P.W.S. Heng, L.W. Chan, Alginates as a useful natural polymer for microencapsulation and therapeutic

applications, Carbohydrate Polymers, 88 (2012) 1-12.
[20] A. Veronovski, Z. Knez, Z. Novak, Preparation of multi-membrane alginate aerogels used for drug delivery, J Supercrit Fluid, 79 (2013) 209-215.
[21] U. Dashdorj, M.K. Reyes, A.R. Unnithan, A.P. Tiwari, B. Tumurbaatar, C.H. Park, C.S. Kim, Fabrication and characterization of electrospun zein/Ag nanocomposite mats for wound dressing applications, Int J Biol Macromol, 80 (2015) 1-7.
[22] C.Y. Wang, H.X. Liu, Q.X. Gao, X.X. Liu, Z. Tong, Alginate-calcium carbonate porous microparticle hybrid hydrogels with versatile drug loading capabilities and variable mechanical strengths, Carbohydrate Polymers, 71 (2008) 476-480.
[23] M. Nawaz, W. Miran, J. Jang, D.S. Lee, One-step hydrothermal synthesis of porous 3D reduced graphene oxide/TiO2 aerogel for carbamazepine photodegradation in aqueous solution, Appl Catal B: Environ, 203 (2017) 85-95.
[24] J.D. Zhuang, Q.F. Tian, S. Lin, W.B. Yang, L.H. Chen, P. Liu, Precursor morphology-controlled formation of perovskites CaTiO3 and their photo-activity for As(III) removal, Appl Catal B: Environ, 156 (2014) 108-115.
[25] J. Zhuang, W. Dai, Q. Tian, Z. Li, L. Xie, J. Wang, P. Liu, X. Shi, D. Wang, Photocatalytic degradation of RhB over TiO2 bilayer films: effect of defects and their location, Langmuir, 26 (2010) 9686-9694.
[26] F. Sordello, G. Zeb, K.W. Hu, P. Calza, C. Minero, T. Szkopek, M. Cerruti, Tuning TiO2 nanoparticle morphology in graphene-TiO2 hybrids by graphene surface modification, Nanoscale, 6 (2014) 6710-6719.
[27] M. Nawaz, M. Moztahida, J. Kim, A. Shahzad, J. Jang, W. Miran, D.S. Lee, Photodegradation of microcystin-LR using graphene-TiO2/sodium alginate aerogels, Carbohydrate Polymers, 199 (2018) 109-118.
[28] J. Phiri, L.S. Johansson, P. Gane, T. Maloney, A comparative study of mechanical, thermal and electrical properties of graphene-, graphene oxide- and reduced graphene oxide-doped microfibrillated cellulose nanocomposites, Compos Part B: Eng, 147 (2018) 104-113.
[29] R.X. Ma, Y.J. Wang, H.J. Qi, C. Shi, G.B. Wei, L.D. Xiao, Z.H. Huang, S.X. Liu, H.P. Yu, C.B. Teng, H. Li, V. Murugadoss, J.X. Zhang, Y.G. Wang, Z.H. Guo, Nanocomposite sponges of sodium alginate/graphene oxide/polyvinyl alcohol as potential wound dressing: In vitro and in vivo evaluation, Compos Part B: Eng, 167 (2019) 396-405.
[30] L. Sun, B. Fugetsu, Graphene oxide captured for green use: Influence on the structures of calcium alginate and macroporous alginic beads and their application to aqueous removal of acridine orange, Chem Eng J, 240 (2014) 565-573.
[31] A.C. Ferrari, S.E. Rodil, J. Robertson, Interpretation of infrared and Raman spectra of amorphous carbon nitrides, Phys Rev B, 67 (2003) 155306.
[32] J.C. Wang, S.A. Kondrat, Y.Y. Wang, G.L. Brett, C. Giles, J.K. Bartley, L. Lu, Q. Liu, C.J. Kiely, G.J. Hutchings, Au-Pd Nanoparticles Dispersed on Composite Titania/Graphene Oxide-Supports as a Highly Active Oxidation Catalyst, Acs Catal, 5 (2015) 3575-3587.
[33] H.L. Wang, J.T. Robinson, X.L. Li, H.J. Dai, Solvothermal Reduction of Chemically Exfoliated Graphene Sheets, J Am Chem Soc, 131 (2009) 9910-9911.
[34] B.C. Qiu, Q.Y. Li, B. Shen, M.Y. Xing, J.L. Zhang, Stober-like method to synthesize ultradispersed Fe3O4 nanoparticles on graphene with excellent Photo-Fenton reaction and high-performance lithium storage, Appl Catal B: Environ, 183 (2016) 216-223.
[35] J. Liu, P. Li, L. Chen, Y. Feng, W.X. He, X.H. Yan, X.M. Lu, Superhydrophilic and underwater superoleophobic modified chitosan-coated mesh for oil/water separation, Surf Coat Tech, 307 (2016) 171-176.
[36] J. Yang, L.T. Yin, H. Tang, H.J. Song, X.N. Gao, K. Liang, C.S. Li, Polyelectrolyte-fluorosurfactant complex-based meshes with superhydrophilicity and superoleophobicity for oil/water separation, Chem Eng J, 268 (2015) 245-250.
[37] Y.Q. Liu, Y.L. Zhang, X.Y. Fu, H.B. Sun, Bioinspired Underwater Superoleophobic Membrane Based on a Graphene Oxide Coated Wire Mesh for Efficient Oil/Water Separation, Acs Appl Mater Inter, 7 (2015) 20930-20936.
[38] Z.X. Xue, S.T. Wang, L. Lin, L. Chen, M.J. Liu, L. Feng, L. Jiang, A Novel Superhydrophilic and Underwater

Superoleophobic Hydrogel-Coated Mesh for Oil/Water Separation, Adv Mater, 23 (2011) 4270-4273.
[39] K.S. Hu, D.D. Kulkarni, I. Choi, V.V. Tsukruk, Graphene-polymer nanocomposites for structural and functional applications, Prog Polym Sci, 39 (2014) 1934-1972.
[40] J.H. Liu, U. Khan, J. Coleman, B. Fernandez, P. Rodriguez, S. Naher, D. Brabazon, Graphene oxide and graphene nanosheet reinforced aluminium matrix composites: Powder synthesis and prepared composite characteristics, Mater Design, 94 (2016) 87-94.
[41] Y. Cai, Q.H. Lu, X.L. Guo, S.T. Wang, J.L. Qiao, L. Jiang, Salt-Tolerant Superoleophobicity on Alginate Gel Surfaces Inspired by Seaweed (Saccharina japonica), Adv Mater, 27 (2015) 4162-4168.
[42] G.D. Carbohydrate PolymersAcs NanoCarbohydrate PolymersBixler, B. Bhushan, Biofouling: lessons from nature, Philos T R Soc A, 370 (2012) 2381-2417.
[43] Y. Si, Q.X. Fu, X.Q. Wang, J. Zhu, J.Y. Yu, G. Sun, B. Ding, Superelastic and Superhydrophobic Nanofiber-Assembled Cellular Aerogels for Effective Separation of Oil/Water Emulsions, Acs Nano, 9 (2015) 3791-3799.
[44] W.B. Zhang, Y.Z. Zhu, X. Liu, D. Wang, J.Y. Li, L. Jiang, J. Jin, Salt-Induced Fabrication of Superhydrophilic and Underwater Superoleophobic PAA-g-PVDF Membranes for Effective Separation of Oil-in-Water Emulsions, Angew Chem Int Edit, 53 (2014) 856-860.
[45] V. Hejazi, M. Nosonovsky, Wetting Transitions in Two-, Three-, and Four-Phase Systems, Langmuir, 28 (2012) 2173-2180.